17th World Conference on Earthquake Engineering, 17WCEE
Sendai, Japan - September 13th to 18th 2020

COMPARISON OF E-DEFENSE TEST RESULTS BY FIVE INSTITUTES OF SEMI-ACTIVE CONTROL OF BASE-ISOLATION SYSTEM

H. Fujitani[(1)], Y. Mukai[(2)], E. Sato[(3)], E. A. Johnson[(4)], R. Christenson[(5)], A. Kishida[(6)], M. Ito[(7)]
T. Shima[(8)], K. Itahara[(9)], S. Iba[(10)], A. Honma[(11)], H. Fukui[(12)]

(1) Professor, Graduate School of Engineering, Kobe University, fujitani@kobe-u.ac.jp
(2) Associate Professor, Graduate School of Engineering, Kobe University, ymukai@port.kobe-u.ac.jp
(3) Senior Researcher, National Research Institute of Earth Science and Disaster Resilience, eiji@bosai.go.jp
(4) Professor, Department of Civil and Environmental Engineering, University of Southern California, johnsone@usc.edu
(5) Professor, Department of Civil and Environmental Engineering, University of Connecticut, rchriste@engr.uconn.edu
(6) Researcher, National Research Institute of Earth Science and Disaster Resilience, akiko_kishida@bosai.go.jp
(7) Senior Research Engineer, Building Research Institute, mai_ito@kenken.go.jp
(8) Student, Department of Architecture, Kobe University, 1664021t@stu.kobe-u.ac.jp
(9) Graduate Student, Department of Architecture, Kobe University, 185t005t@stu.kobe-u.ac.jp
(10) Graduate Student, Department of Architecture, Kobe University, 180t008t@stu.kobe-u.ac.jp
(11) Graduate Student, Department of Architecture, Kobe University, 194t042t@stu.kobe-u.ac.jp
(12) Ph. D. Student, Department of Architecture, Kobe University, 153t049t@stu.kobe-u.ac.jp

Abstract

Large-scale shaking table tests were conducted to assess semi-active control of base-isolation systems. Researchers from three universities and two institutes in Japan and the United States proposed semi-active control strategies designed to prevent excessive deformation of base-isolation systems under near-fault pulse ground motions, specifically the Takatori ground motion of the 1995 Southern Hyogo prefecture Earthquake, the Sylmar ground motion of the 1994 Northridge Earthquake, and the El Centro ground motion of the 1940 Imperial Valley Earthquake. They examined semi-active control strategies not only in terms of reducing isolation deformation but also of preventing increased floor acceleration to maintain building functions. The adopted semi-active control methods were designed independently for these tests or were arranged based on LQR control, Sliding mode control, Fuzzy control, and Sky-hook control. The authors verified the efficacy of the proposed control methods using shaking table tests of E-Defense with a large-scale base-isolated building model and a magneto-rheological fluid damper (MR damper).

Test results of all the semi-active strategies were mutually compared to assess aspects of passive strategies: low friction damping, intermediate-viscosity damping (20%), high-viscosity damping (30%), and high-friction damping. Comparisons were conducted from the perspective of (a) reduction of maximum displacements of base-isolation, (b) reduction of maximum and RMS values of floor accelerations of the superstructure, (c) equivalent viscous damping factor, (d) damping performance evaluation with response displacements and accelerations, and so on.

Comparisons yielded up-to-date knowledge of which semi-active control method is most effective to reduce response displacement and which method is effective to reduce superstructure floor acceleration against near-fault pulse ground motions along with test results for common conditions.

Keywords: Base-isolation; E-Defense test; Near fault pulse ground motion; Semi-active control strategy

1. Introduction and Objectives

Protecting structures from extremely large ground motions is an important task of structural engineering. Even base isolation systems might cause large deformation in the base-isolation layer, especially because of near fault pulse ground motions. In such cases, semi-active control is probably effective to reduce not only deformation but also floor acceleration to maintain building structure functions. For that purpose, a series of large-scale shaking table tests were conducted for semi-active control of base-isolation systems [1]. Researchers from five institutes in US and Japan worked on the same target by their own control method using a magneto-rheological fluid damper (MR damper). For this study, some test results obtained using representative control strategies and some discussions were conducted from the perspective of damping effects to both the deformation of base isolation and absolute accelerations of the superstructure. Finally, the semi-active control strategy effectiveness and important factors affecting it are discussed.

2. Test specimena

For this study, shaking table tests for the semi-active isolation structure as presented in Fig. 1 and Photo 1 were conducted using an MR damper as presented in Photo 2. The superstructure of the semi-active isolation structure is 6000(W) × 4500(D) × 2300(H): an approximately 14.9 ton steel frame structure. The superstructure was supported by linear guides. A natural rubber bearing was installed between the superstructure and the shaking table. An MR damper was used for the variable damper. The target response of the superstructure is realized by controlling the damping force of the MR damper. The isolation performance for the semi-active isolation system was evaluated from the E-Defense shaking tests using various earthquake groundmotions.

Stiffness of the base isolation system by a natural rubber bearing is 42.3 kN/m, which is the average value of cyclic loading tests in the displacement amplitude from 75 mm to 200 mm. The natural period of the base isolation system is 3.73 s, ignoring damping effects. Then, damping factor of the base isolation system from the roller bearing and natural rubber bearing was estimated as about 19% by the shaking table test. The MR damper capacity is about 10 kN by application of 5.0 A electric current. Fig. 2 shows the damper force - displacement relation and damper force – piston velocity relation of the MR damper. The MR damper was modeled by every reserachers according to the contol method.

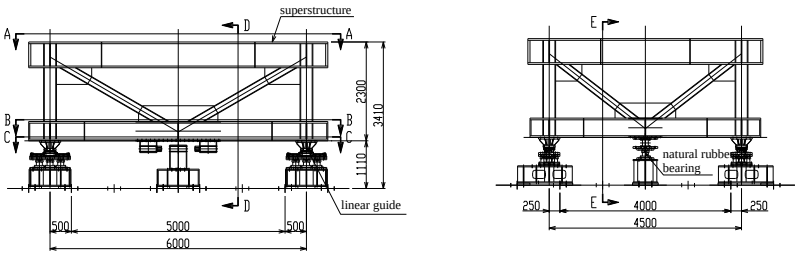

Fig.1 – Drawing of semi-active seismic isolation

Photo 1 – Schematic view of E-Defense test

Photo 2 – MR damper installed in the base isolation layer

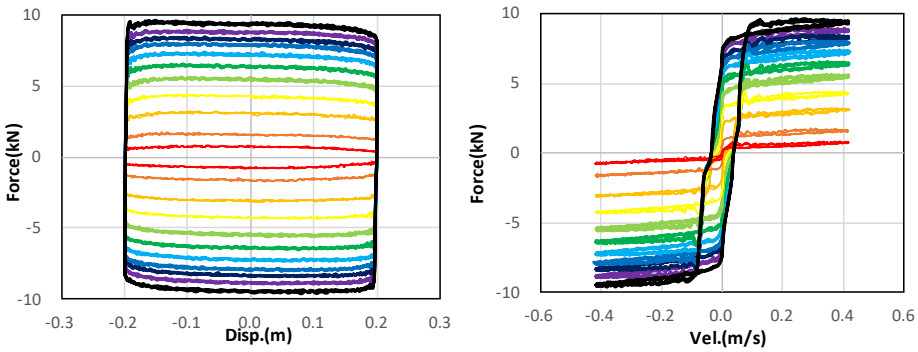

Fig.2 – Damper force – displacement and velocity relation of MR damper by sinusoidal excitation ±200 mm 0.33 Hz

Damping effect of the base isolation has to be evaluated, because damping effects are discussed in Chapter 4. This test specimen has one rubber bearing and four roller bearings. The horizontal force of every bearing was measured by the load cell. In this section, the equivalent damping coefficient was calculated as the inclination of the relation of force and velocity. Then the equivalent damping factor is calculated. The results are presented in Table 1. For this evaluation, the restoring force of the rubber bearing was calculated by multiplying the rubber bearing stiffness by the relative displacement, and was subtracted the measured force.

Table 1 - Damping effect of the base isolation layer by one natural rubber bearing and four roller bearings

Earthquake groundmotions	Equivalent damping coefficient (kN・s/m)	Equivalent damping factor (%)
El Centro 1940 NS	10.504	20.94
JR Takatori 1995 NS	10.202	20.34
Sylmar 1994 NS	7.9426	15.83
Average	9.5495	19.04

3. Semi-active Control Strategy

All participants proposed their control strategies. The response reduction effects were mutually compared and were compared with passive viscous damping. Table 2 presents names for all of the test cases. Nos. 1 - 3 are the passive viscous damping cases, as controlled by the MR damper so that the damper force is nearly equal to that which is proportional to the piston velocity. The target damping factors were 10%, 20%, and 30%. No. 4 presents the hard breaking test case in which 4 A electric current is applied to the MR damper through the shaking test. No. 5 is the soft damping test case without application of electric current.

Here, some semi-active control strategies are introduced. Then they are mutually compared.

[No. 6] State feedback optimal control

[No.8] LQR considering restoring force (Kobe University) [2][3]

Eq. (1) shows the equation of motion of the absolute coordinate system of one mass system.

$$\mathrm{m}(\ddot{x}+\ddot{z})+c(\dot{x}+\dot{z})+\mathrm{k}(\mathrm{x}+\mathrm{z})=\mathrm{c}\dot{z}+kz \tag{1}$$

Table 2 – Test cases

1. 10% viscous damping	2. 20% viscous damping	3. 30% viscous damping
4. Passive_on (4A applied)	5. Passive_off (without electric current)	6. State feedback optimal control
7. LQR considering ground motion	8. LQR considering restoring force	9. State feedback EF Control considering restoring force
10. Complex stiffness control	11. Velocity proportional control	12. Energy function control
13. SlidingModeControl_LQR_Gd10Gv1	14. SlidingModeControl_LQR_Gd10Gv10	15. SlidingModeControl_LQR_Gd100Gv10_CLIP
16. BRI_Sliding mode_1	17. BRI_Sliding mode_2	18. NIED_LQ(PI)_1
19. NIED_LQ(PI)_2	20. NIED_variable hydraulic damper_1	21. NIED_variable hydraulic damper_2
22. USC_1_CLQR_nounitdelay	23. USC_2_OCLCelcentro_nounitdelay	24. USC_3_OCLCnorthridge_nounitdelay
25. USC_3_OCLCnorthridge_3state_4A	26. USC_6_OCLCnorthridge_new_controller_4A	27. UConn_Fuzzy
28. UConn_Fuzzy2	29. UConn_Friction	30. UConn_Skyhook
31. UConn_VelocityPH		

Each gain is determined using the evaluation function of the Eq. (2). The MR damper exerts the optimum control force.

$$J = \frac{1}{2}\int (\boldsymbol{Y}^T \boldsymbol{Q}\boldsymbol{Y} + ru^2)dt \tag{2}$$

$$\boldsymbol{Q} = \begin{bmatrix} \alpha_d & 0 & 0 \\ 0 & \alpha_v & 0 \\ 0 & 0 & \alpha_a \end{bmatrix}, \alpha_d \cdot \alpha_v \cdot \alpha_a \cdot u : \text{Weight coefficient}$$

If the right side of Eq. (2) becomes zero, then it is considered that the one mass system does not move in the absolute coordinate system. The damping force F_d might be applied so that the right side becomes zero.

$$m(\ddot{x} + \ddot{z}) + c(\dot{x} + \dot{z}) + k(x + z) = c\dot{z} + kz - F_d = 0 \tag{3}$$

$$F_d = c\dot{z} + kz \tag{4}$$

The restoring force F_d, optimal control, and feedback control are combined. The feedback control purpose is to show effects of ground motion observation errors and disturbances.

[No.10] Control system simulating the complex stiffness damper (Kobe University) [4][5]

A control strategy that simulates the complex stiffness damper using an MR damper is proposed. Eq. (5) shows the equation of motion for a single degree of freedom system that represents a base-isolated building whose isolation layer has a complex stiffness damper. Eq. (6) shows the damping force.

$$m\ddot{x} + (k + 2\beta ki)x = -m\ddot{x}_g \tag{5}$$

$$f_c(t) = 2\beta kix(t) = 2\beta kiXe^{i\omega t} \tag{6}$$

In those eauations, m is the lumped mass, k is the stiffness, x is the response displacement, x_g is the ground displacement, β is the complex damping factor, f_c is the damping force of the complex stiffness damper, and i represents the imaginary unit. It might be readily apparent from Eq. (6) that the complex stiffness damper is independent of the frequency and that is outputs the force proportional to the displacement amplitude. The multiplication of imaginary unit i in Eq. (6) means that the damper force is $\pi/2$ forward of the response displacement in the frequency domain. Obtaining displacement 1/4 of natural period later (the phase is let be $\pi/2$ forward) solely from only information is impossible at present. The complex stiffness damper hsas no causal relation in the time domain. As shown in Eq. (5), the damping force of the complex stiffness damper f_c can be introduced from that of the passive viscous damper f_v as

$$f_c = (\omega_0/\omega)f_v \tag{7}$$

where f_v represents the damping force of the passive viscous damper, ω is the natural circular frequency of ground motion, and ω_0 is the the natural circular frequency of the lumped mass system.

The transformation of Eq. (7) is the target transformation. The digital filter is used for simulation.

[No.16] BRI Sliding mode_1 (Building Research Institute) [6]

In sliding mode control, a switching hyperplane and a sliding mode controller are designed to ensure that the trajectories of the system move toward the hyperplane and slide along the surface to the origin. An eventual sliding mode control scheme, which consists of two independent terms, namely, a linear control term and a non-linear control term, was employed for the tests. To reduce the chattering of the control signal, which is a harmful high frequency excitation, a smoothing function was used for the non-linear control term. The gains of the non-linear control term, which were 4000 and 8000, were adopted as the test parameters.

[No.20] Switching damping coefficient (National Institute of Earth Science and Disaster Resilience) [3]

A semi-active hydraulic damper was assumed to switch damping coefficient to two phases. The authors set two damping coefficients equivalent to 10% and 30% damping factors: c_L and c_H. The ideal control force was calculated using LQ theory. As one method, the damping coefficient can be set to c_H when the output force of the damper becomes smaller than the ideal control force. Alternatively, the damping coefficient is set as c_L when the output force becomes greater than or equal to the ideal control force. However, this method causes chattering. To prevent chattering, we adopted the original strategy by which the damping coefficient keeps c_L, whereas the velocity direction is the same, after the output force of the damper once becomes greater than or equal to the ideal control force and the damping coefficient is switched to c_L.

[No.25] USC_5_A three-state_OCLC northridge_new_controller_4A (University of Southern California) [7][8]

Optimal clipped linear control (OCLC), a novel state feedback control strategy proposed by Fang and Johnson et al. [1], is designed by optimizing, given a design excitation, a quadratic cost metric for the nonlinear system with consideration of the controllable damper. Two different objective functions (J1 and J2) are investigated for controller design: J1 is the summation of weighted mean square displacement, velocity, absolute accelerations and control force; while J2 is the summation of weighted mean square displacement, absolute accelerations, and mass-normalized control force.

[No.29] UConn_Friction (University of Connecticut) [9]

The modulated homogeneous friction control strategy is a relatively straightforward control. The desired current applied to the damper is equal to a peak value of relative displacement across the damper (i.e., when the relative velocity across the damper is zero) multiplied by a gain constant. The control law is:

$$i_{cmd}(t)=g\times|P[x_{rel}(t)]| \tag{8}$$

$$g \cong \frac{i_{max}}{x_{rel}^{max}} \tag{9}$$

where g is a positive gain, based on a maximum applied current for a set relative displacement.

4. Comparison of Test Results

4.1 Input earthquake ground motions

Those ground motions were input to the shaking table by adjusting the acceleration amplitude.

1) El Centro 1940 NS; accelerations are multiplied by 1.5 times.
2) JR Takatori 1995 NS; accelerations are multiplied by 0.4 times.
3) Sylmar 1994 NS; accelerations are multiplied by 0.5 times.

4.2 Comparison of test results in maximum displacements and RMS of the floor accelerations

Figs. 3 and 4 show the maximum response displacements and floor accelerations or RMS values of the floor accelerations.

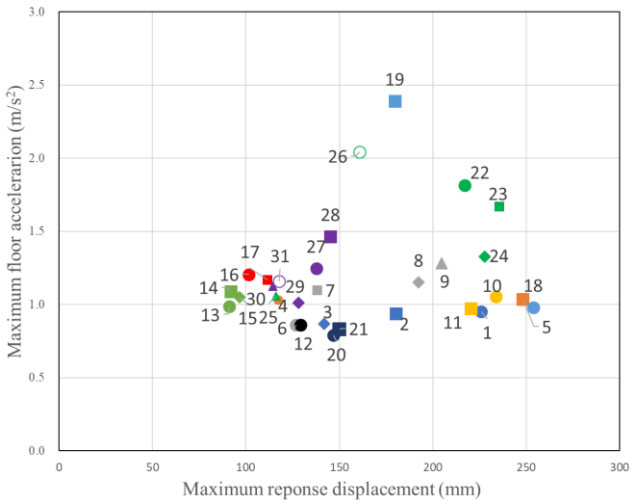

(a) El Centro 1940 NS 150 %

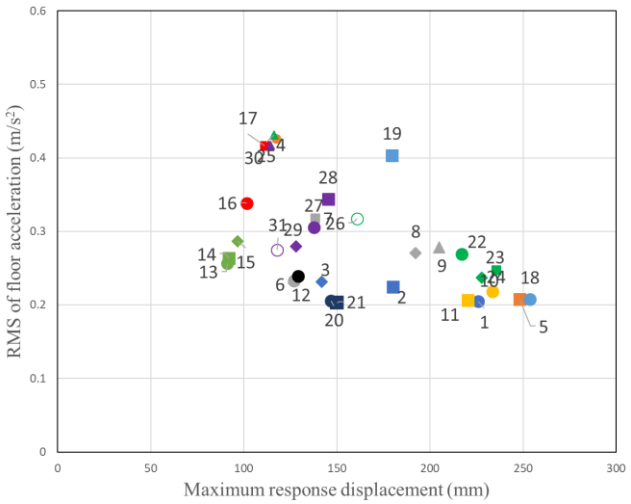

(a) El Centro 1940 NS 150 %

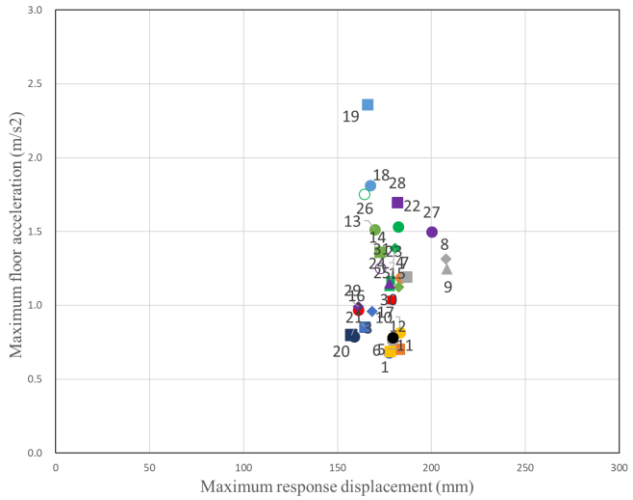

(b) Takatori 1995 NS 40 %

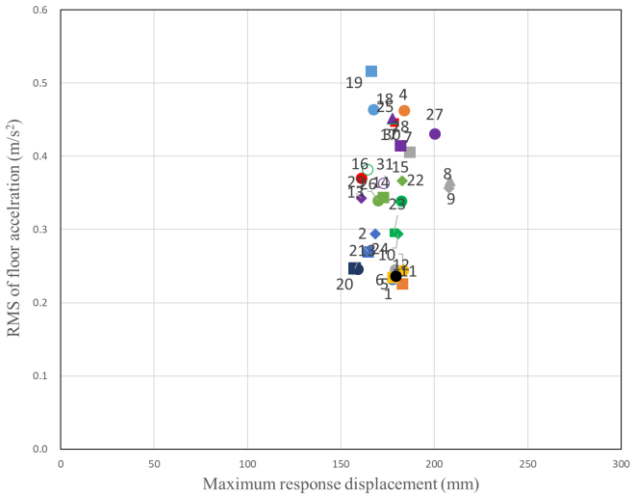

(b) Takatori 1995 NS 40 %

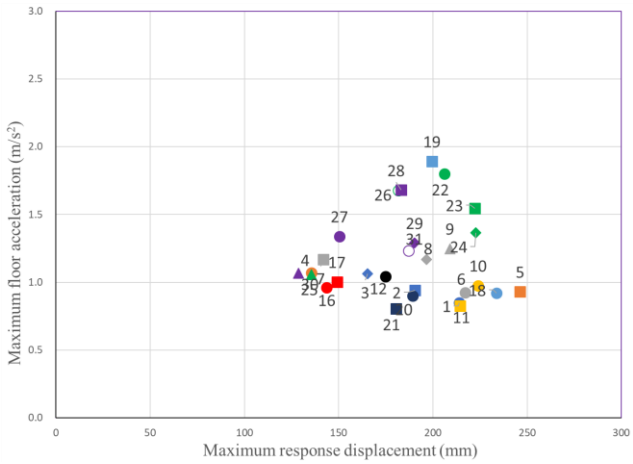

(c) Sylmar 1994 NS 50 %

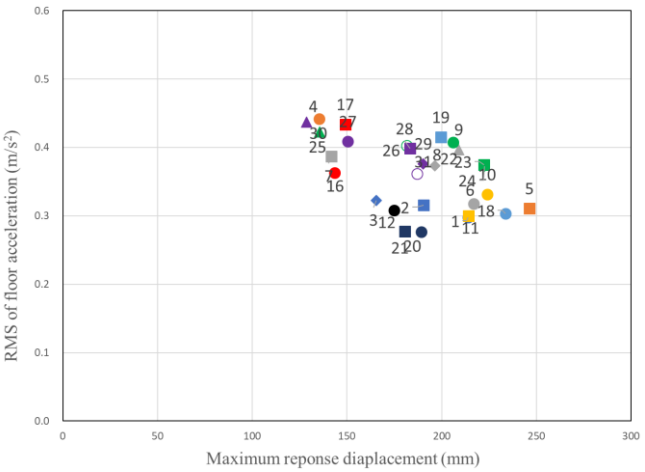

(c) Sylmar 1994 NS 50 %

Fig. 3 – Relation of maximum floor acceleration and maximum response displacement

Fig. 4 – Relation of RMS of floor acceleration and maximum response displacement

4.3 Evaluation of MR damper effects

The damping effects of the MR damper are evaluated next. The damping effect is expressed by the equivalent damping coefficient by MR damper C_{MR} (kN・s/m) and the equivalent damping factor by MR damper h_{MR} (%). Fig. 4 shows that the C_{MR} is derived as the inclination of linear function approximated using least squares method from the relation of the damping force of MR damper and the piston velocity. Then, the equivalent damping factor h_{MR} is calculated. Results of every excitation are presented in Table 4. The average values of C_{MR} and h_{MR} of every controller in the three ground motions are also presented in Table 4.

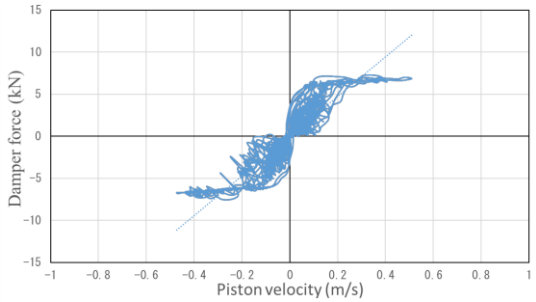

Fig.4 – Relation of the damping force of MR damper and piston velocity (El Centro, Controller No. 6)

From results presented in Table 4, one can observe the following. In the test cases (1) - (3), the equivalent damping factors h_{MR} were, respectively 6.4, 14.0, and 22.1%, although the target damping factor was 10-30% in the damping factor. In the test cases (4) and (5), the equivalent damping factor h_{MR} was 55.0% by continuous application of 4A electric current, and 3.3% without electric current. The relation between the equivalent damping factor h_{MR} and the response reduction effect is discussed in the following section.

4.4 Evaluation of response reduction by semi-active control by MR damper

This section presents evaluation of the damping effect of semi-active control by MR damper from some perspectives as explained below.

1) The relationship between equivalent damping factor h_{MR} and non-dimensional displacement *R*d was found.
→Fig.6.
2) The relation between the equivalent damping factor h_{MR} and the length of the straight line binding the origin and the plot of every controlled response in the coordinate plane of the non-dimensional displacement *R*d and the non-dimensional acceleration *R*a is presented in Fig. 5 [10]. This figure shows the response reduction effects of both displacement and acceleration. Here, *R*d denotes the ratio of maximum response displacement divided by that in a case of "Passive off (without application of the electric current)". Also, *R*a is the ratio of maximum absolute acceleration of the superstructure divided by that in the case of "Passive off".
→Fig.7.

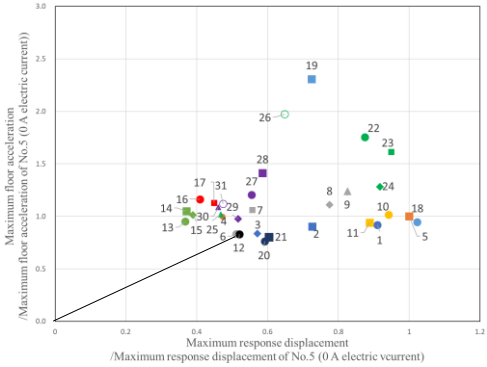

Fig. 5 - Straight line binding the origin and the plot of every controlled response and the angle

Table 4 – Equivalent damping coefficient C_{MR} (kN·s/m) and equivalent damping factor h_{MR} (%) by MR damper

Test case (Control method)	Equivalent damping coefficient C_{MR} (kN·s/m)				Equivalent damping factor h_{MR} (%)			
	El Centro	Takatori	Sylmar	Average	El Centro	Takatori	Sylmar	Average
(1) 10% viscous damping	3.35	3.24	3.02	3.20	6.67	6.46	6.02	6.38
(2) 20% viscous damping	7.08	6.95	7.04	7.02	14.12	13.85	14.04	14.00
(3) 30% viscous damping	11.15	11.09	11.05	11.10	22.22	22.10	22.03	22.12
(4) Passive_on (4A applied)	32.40	26.22	24.18	27.60	64.59	52.27	48.02	54.96
(5) Passive_off (0A applied)	1.82	1.64	1.43	1.63	3.63	3.26	2.85	3.25
(6) State feedback optimal control	12.32	3.30	3.18	6.27	24.56	6.58	6.34	12.49
(7) LQR considering ground motion	23.59	22.79	20.93	22.44	47.02	45.43	41.72	44.72
(8) LQR considering restoring force	10.17	10.49	9.54	10.07	20.28	20.90	19.02	20.07
(9) State feedback EF control considering restoring force	9.42	9.45	8.76	9.21	18.78	18.83	17.45	18.35
(10) Complex stiffness control	2.68	2.57	2.56	2.60	5.34	5.11	5.11	5.19
(11) Velocity proportional control	3.79	3.72	3.55	3.69	7.55	7.42	7.07	7.35
(12) Energy function (EF) control	13.21	3.30	9.38	8.63	26.33	6.58	18.70	17.20
(13) Sliding mode control_ LQR_Gd10Gv1	20.27	18.48	-	19.37	40.40	36.85	-	38.63
(14) Sliding mode control_ LQR_Gd10Gv10	19.39	18.63	-	19.01	38.66	37.13	-	37.90
(15) Sliding mode control_ LQR_Gd100Gv10_CLIP	22.53	19.93	-	21.23	44.91	39.74	-	42.33
(16) BRI_Sliding mode_1	24.90	20.46	16.96	20.77	49.64	40.79	33.81	41.41
(17) BRI_Sliding mode_2	28.35	23.49	20.90	24.25	56.87	46.82	41.66	48.45
(18) NIED_LQ(PI)_1	1.64	4.33	1.38	2.45	3.28	8.63	2.74	4.88
(19) NIED_LQ(PI)_2	8.29	4.06	6.772	6.37	16.53	8.08	13.50	12.70
(20) NIED_variable hydraulic damper_1	7.90	7.72	7.39	7.67	15.75	15.38	14.73	15.29
(21) NIED_variable hydraulic damper_2	8.47	8.31	8.10	8.29	16.89	16.56	16.14	16.53
(22) USC_1_CLQR_ nounitdelay	3.09	2.90	2.83	2.94	6.15	5.78	5.63	5.85
(23) USC_2_OCLC elcentro_nounitdelay	2.46	2.45	2.18	2.36	4.90	4.87	4.34	4.70
(24) USC_3_OCLC northridge_nounitdelay	2.56	2.51	2.21	2.42	5.10	5.01	4.40	4.84
(25) USC_3_OCLC northridge_3state_4A	32.75	25.17	23.36	27.09	65.28	50.18	46.56	54.01
(26) USC_6_OCLC northridge_new_controller_4A	5.09	4.69	5.06	4.95	10.14	9.36	10.08	9.86
(27) UConn_Fuzzy	15.71	14.85	14.74	15.10	31.31	29.60	29.39	30.10
(28) UConn_Fuzzy2	16.13	13.92	12.58	14.21	32.16	27.75	25.08	28.33
(29) UConn_Friction	19.01	16.36	14.76	16.71	37.89	32.60	29.42	33.30
(30) UConn_Skyhook	32.57	25.91	24.47	27.65	64.93	51.65	48.77	55.12
(31) UCcnn_VelocityPH	12.78	11.27	10.53	11.52	25.47	22.46	20.98	22.97

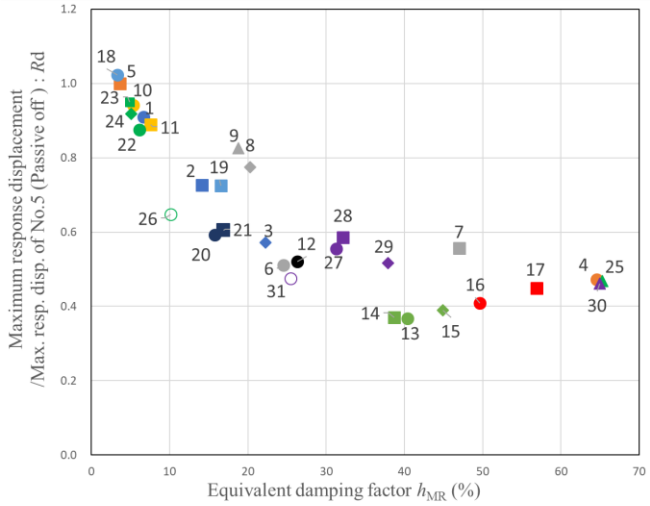

(a) El Centro 1940 NS 150 %

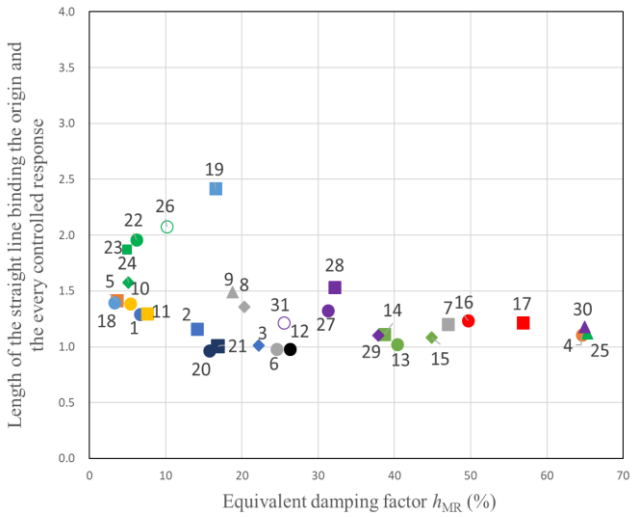

(a) El Centro 1940 NS 150 %

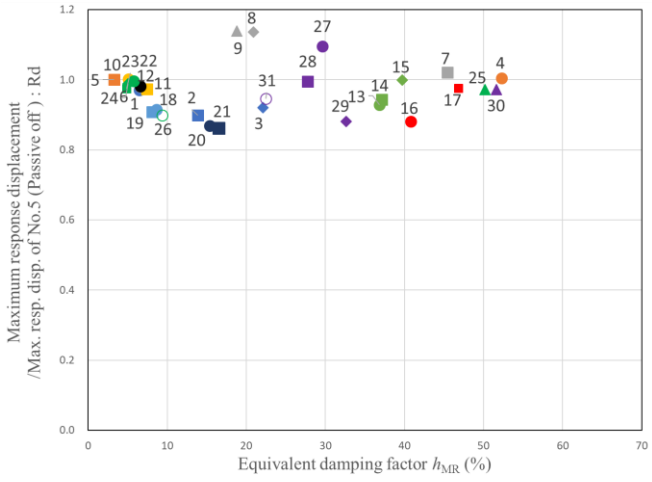

(b) Takatori 1995 NS 40 %

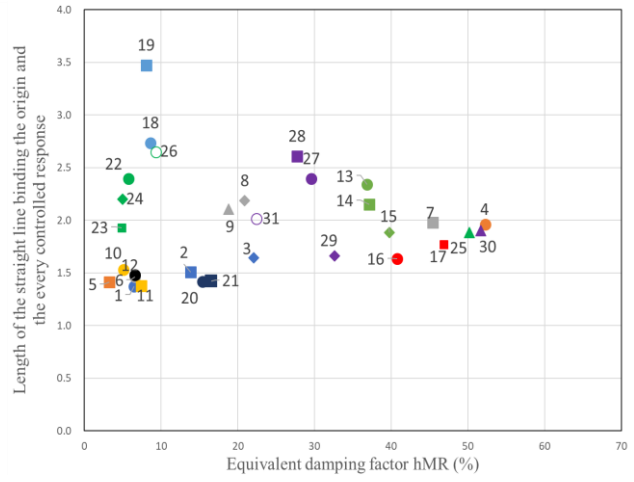

(b) Takatori 1995 NS 40 %

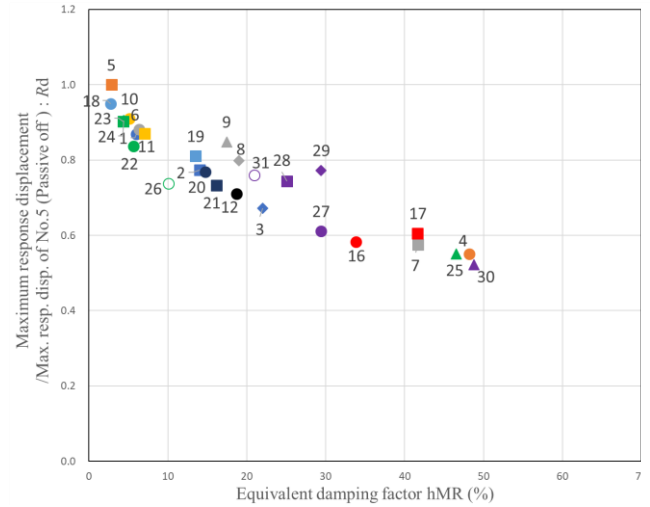

(c) Sylmar 1994 NS 50 %

Fig. 6 - Relation of non-dimensional displacement *R*d and equivalent damping coefficient

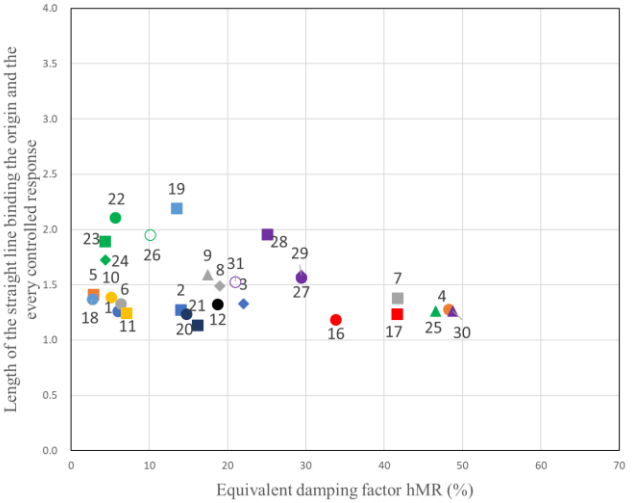

(c) Sylmar 1994 NS 50 %

Fig.7 – Relation of length from the origin and equivalent damping coefficient

Table 5 – The non-dimensional displacement *R*d and the non-dimensional acceleration *R*a

	El Centro				Takatori				Sylmar			
	h_{MR} (%)	*R*d	*RMS of* Acc	Length	h_{MR}	*R*d	*RMS of* Acc	Length	h_{MR} (%)	*R*d	*RMS* of Acc	Length
0A	3.63	1.000	0208	1.000	3.26	1.000	0.226	1.000	2.85	1.000	0.311	1.000
4A	64.59	0.472	0.426	0.781	52.27	1.004	0.463	1.387	48.02	0.550	0.441	0.590
10%	6.67	0.911	0.205	0.914	6.46	0.971	0.232	0.969	6.02	0.869	0.298	0.871
20%	14.12	0.726	0.224	0.820	13.85	0.899	0.270	1.068	14.04	0.774	0.316	0.788
30%	22.22	0.571	0.232	0.717	22.10	0.921	0.294	1.164	22.03	0.672	0.322	0.704
No. 6	24.56	0.511	0.233	0.691	6.58	0.979	0.245	1.034	6.34	0.881	0.318	0.885
No. 7	47.02	0.557	0.318	0.848	45.43	1.021	0.406	1.399	41.72	0.576	0.387	0.625
No. 8	20.28	0.775	0.27	0.958	20.9	1.136	0.356	1.546	19.02	0.798	0.373	0.822
No. 9	18.78	0.826	0.278	1.053	18.83	1.139	0.366	1.49	17.45	0.849	0.397	0.876
No.10	5.34	0.942	0.218	0.98	5.11	1.002	0.245	1.083	5.11	0.91	0.331	0.916
No.11	7.55	0.889	0.206	0.915	7.42	0.973	0.235	0.975	7.07	0.87	0.3	0.872
No.12	26.33	0.521	0.239	0.693	6.58	0.981	0.237	1.048	18.7	0.71	0.308	0.735
No.13	40.4	0.368	0.256	0.722	36.85	0.929	0.34	1.657	-	-	-	-
No.14	38.66	0.371	0.263	0.787	37.13	0.943	0.344	1.522	-	-	-	-
No.15	44.91	0.389	0.287	0.767	39.74	0.999	0.367	1.332	-	-	-	-
No.16	49.64	0.409	0.339	0.872	40.79	0.88	0.371	1.156	33.81	0.583	0.363	0.611
No.17	56.87	0.449	0.416	0.859	46.82	0.976	0.447	1.251	41.66	0.606	0.434	0.634
No.18	3.28	1.023	0.208	0.986	8.63	0.915	0.464	1.935	2.74	0.95	0.303	0.951
No.19	16.53	0.724	0.404	1.71	8.08	0.908	0.517	2.457	13.5	0.81	0.415	0.9
No.20	15.75	0.592	0.206	0.683	15.38	0.868	0.246	1.003	14.73	0.768	0.276	0.779
No.21	16.89	0.605	0.203	0.71	16.56	0.861	0.247	1.006	16.14	0.733	0.277	0.74
No.22	6.15	0.875	0.269	1.386	5.78	0.997	0.339	1.693	5.63	0.837	0.407	0.919
No.23	4.90	0.95	0.248	1.324	4.87	0.974	0.296	1.364	4.34	0.903	0.375	0.95
No.24	5.10	0.918	0.237	1.115	5.01	0.988	0.294	1.557	4.40	0.904	0.373	0.935
No.25	65.28	0.468	0.431	0.794	50.18	0.971	0.451	1.331	46.56	0.55	0.423	0.589
No.26	10.14	0.648	0.317	1.469	9.36	0.898	0.382	1.874	10.08	0.738	0.403	0.82
No.27	31.31	0.555	0.306	0.937	29.6	1.095	0.431	1.694	29.39	0.611	0.409	0.677
No.28	32.16	0.586	0.344	1.082	27.75	0.995	0.414	1.845	25.08	0.744	0.399	0.821
No.29	37.89	0.517	0.28	0.78	32.6	0.88	0.343	1.175	29.42	0.773	0.376	0.807
No.30	64.93	0.461	0.417	0.834	51.65	0.971	0.452	1.345	48.77	0.522	0.437	0.567
No.31	25.47	0.475	0.275	0.86	22.46	0.945	0.363	1.425	20.98	0.759	0.362	0.792

5. Discussion

In this chapter, the damping effect of semi-active control by MR damper is evaluated from results presented in Chapter 4.

5.1 Maximum response values and RMS values of the absolute accelerations of the superstructure

Fig. 3 shows that the maximum response displacements were reduced well by semi-active control in the case of El Centro without increase of the acceleration. However, for near fault pulse ground motions Takatori and Sylmar, the acceleration increased when the displacement was reduced. Especially in Takatori, the response displacements are not reduced. Nevertheless the accelerations increased by semi-active control. The maximum accelerations in "Passive on" are larger than those of "Passive off" and semi-active control, and RMS values of accelerations in "Passive on" are rather larger than those of "Passive off" (Fig. 4). Performance of the base isolation system is important to reduce the accelerations and maintain building functions during ground excitation. Therefore, control Nos. 6, 20, and 29 for El Centro and control Nos. 20 and 29 for Takatori have good performance. However, for Sylmar, the control Nos. 16 and 25 have superior performance to those of others from the perspective of response reduction without increased acceleration.

5.2 Evaluation of MR damper effects

Table 4 presents MR damper effects with pseudo-passive and semi-active control using the equivalent damping factor h_{MR}. The h_{MR} values are similar in many cases even for different input ground motions. Sometimes, the h_{MR} values differ depending on the input ground motion. For example, control No. 6 has

higher h_{MR} for El Centro and lower h_{MR} for Takatori and Sylmar. Control No. 6 reduces the maximum response displacement well for El Centro. For that reason, the non-dimensional displacement *R*d is smaller (Table 5). Similarly, control Nos. 25 and 29 reduce the maximum response displacement well proportionally to the value of h_{MR}. Furthermore, the RMS values are not always larger, even if h_{MR} is large.

The relation of the equivalent damping factor h_{MR} and the non-dimensional displacement R_d is depicted in Fig. 6. A tendency exists by which the control strategy becoming greater than h_{MR} reduces the response displacement for the El Centro and Sylmar ground motions. However, for Takatori ground motion, the values of non-dimensional displacement R_d are almost identical, irrespective of h_{MR}.

5.3 Total response reduction performance of semi-active control by MR damper

An evaluation method is proposed in section 4.4. The method is according to the idea that the total response reduction performance is evaluated by the reduction effect of both the displacements and the accelerations. The length of the straight line binding the origin and the plot of every controlled response in the coordinate plane of the non-dimensional displacement *R*d and the non-dimensional acceleration *R*a as presented in Fig. 5, represents the total response reduction performance.

The relation between the length of the line and equivalent damping factor h_{MR} is portrayed in Fig. 7. For El Centro ground motion, some plots exist in the left and lower area. Those control strategies are able to reduce both the displacement and the acceleration. For example, control Nos. 6 and 20 can do so. For Takatori ground motion, the length of the line is around 1.000, as shown in Table 5. Therefore, the control effect is not good when compared with passive control. For Sylmar ground motion, a tendency exists by which the plots are lying from the upper left side to the lower right side. Therefore, greater damping capacity is necessary to reduce the responses, for example, control Nos. 16 and 25 presented in Table 5.

6. Conclusions

This study summarized large-scale shaking table test results obtained for semi-active control of the base isolation system by an MR damper using E-Defense. Researchers from five universities and institutes collaborated to ascertain superior control strategies to protect buildings, maintaining safety and the function of the building under extremely large earthquake motions, especially near fault ground motions.

The equivalent damping factor h_{MR} was used to assess response reduction effects achieved using MR dampers. Results show that the control strategy raising larger values of h_{MR} can reduce the response displacements and show that RMS values of accelerations are not always larger, even if h_{MR} is large.

Then, a method for the evaluation of the response reduction performance, using the length of the straight line binding the origin and the plat of every response, was proposed. This method explains the response reduction tendency from the view point of the total response reduction (displacement and acceleration) against earthquake ground motions. However, there is a subject for future study for evaluating the performance of semi-active control.

Finally, the possibility was found of reducing response under near fault pulse ground motions by developing a new control strategy based on the existing fundamental control logic, for example, LQR method and sliding mode method. Developing an evaluation method or prediction of response based on control variables or parameters of the control strategy is our intended subject of future work.

7. Acknowledgements

This work was supported by JSPS Grant No. R2904 in the Program for Fostering Globally Talented Researchers and the research unit of Multidisciplinary Integration for Resilience and Innovation (MIRAI) in Kobe University.

8. References

[1] Sato E, Kishida A, Kajiwara K, Fujitani H, Mukai Y, Ito M, Itahara K, Johnson E, Christenson R (2020): OUTLINE OF E-DEFENSE SHAKING TESTS FOR SEMI-ACTIVE CONTROL OF BASE-ISOLATION SYSTEM. Proceedings of 17th World Conference on Earthquake Engineering, Paper N° C002561.

[2] Itahara K, Fujitani H, Mukai Y, Ito M, Sato E, Iba S (2020): SHAKING TABLE TEST AND REAL-TIME HYBRID SIMULATION IN SEMI-ACTIVE CONTROLLED BASE-ISOLATION SYSTEM. Proceedings of 17th World Conference on Earthquake Engineering, Paper N° C001668.

[3] Yoshida O, Kageyama M, Sano T, Endo F, Watanabe T, Katsumata H (2010): Super Active Base Isolation System "Laputa 2D", *Report of Obayashi Corporation Technical Research Institute*, 74, pp. 1-8. (in Japanese)

[4] Kishida A, Sato E, Iba S, Fujitani H, Mukai Y, Itahara K, Johnson E, Kajiwara K (2020): Semi-active control of base-isolated structure using MR damper that simulates variable hydraulic damper and complex stiffness damper. Proceedings of 17th World Conference on Earthquake Engineering, Paper N° C001644.

[5] Kumagai N, Nakamura S, Ikenaga M, Ikago K, Inoue N (2014): A Study on Implementation of Complex Stiffness Damper for Base Isolated Structure by Using an MR damper. Summaries of Technical Papers of Annual Meeting Architectural Institute of Japan, B-II 495-498 (in Japanese).

[6] Ito M, Fujitani H, Mukai Y, Sato E, Johnson E, Christenson R, Kishida A (2020): EVENTUAL SLIDING MODE CONTROL FOR AN ISOLATED STRUCTURE USING MR DAMPER. Proceedings of 17th World Conference on Earthquake Engineering, Paper N° C001351.

[7] Fang Q, Johnson E, Sato E, Fujitani H, Mukai Y (2020): E-DEFENSE SHAKING TABLE EXPERIMENTS OF CONTROLLABLE DAMPING STRATEGIES FOR A BASE-ISOLATED STRUCTURE. Proceedings of 17th World Conference on Earthquake Engineering, Paper N° C003418.

[8] Fang Q, Johnson E, Brewick PT, Wojtkiewicz SF (2020): Optimal clipped linear strategies for controllable damping. (in preparation), 2018.

[9] Stevens M, Christenson R, ato E, Fujitani H, Mukai Y (2020): PERFORMANCE OF SEMI-ACTIVE CONTROLLERS FOR A LARGESCALE BASE-ISOLATION STRUCTURE WITH MR DAMPER. Proceedings of 17th World Conference on Earthquake Engineering, Paper N° C003370.

[10] Hiwatashi T, Fujitani H (2008): FEASIBILITY STUDY ON SIMPLE QUANTITATIVE APPROACH OF DAMPING PERFORMANCE FOR VARIABLE HYDRAULIC DAMPER. Jounal of Structural and Construction Engineering, AIJ, Vol. 73, No. 629, pp. 1071-1077 (in Japanese).

